Hierarchical parcel-swapping representation of turbulent mixing. III. Origins of correlation patterns observed in turbulent boundary layers

Alan R. Kerstein*
72 Lomitas Road, Danville, California 94526, USA

(Received 24 December 2020; accepted 5 April 2021; published 22 April 2021)

Patterns observed in correlation measurements provided early indications of organized structures in turbulent boundary layers, later supplemented by imaging studies. It is recognized that correlation patterns could in some instances reflect transient flow processes rather than structures, but discrimination among the possible origins of various correlation patterns has not been addressed systematically. Here this is done from three complementary perspectives. First, a conceptual framework termed cascade analogy is shown to imply three processes, all devoid of organized-structure influences, that might induce such patterns. Second, hierarchical parcel swapping (HiPS), a stochastic model that is likewise devoid of such influences, is shown to produce the correlation patterns that are implied by these processes. The HiPS formulation used here is a highly reduced version of a previous formulation, highlighting the elementary nature of the pattern-inducing processes. Third, experimental indications of all these patterns are noted. One pattern, an obliquely oriented ridge of peak cross-correlation between streamwise velocity at various heights and wall stress, is known by other means to be associated with organized structure. The results indicate that the oblique ridge does not in itself uniquely imply this interpretation. This inference is shown to have substantive consequences. The other two patterns are marginally discernible in reported measurements, but there has been no prior assessment of their significance, nor are they obviously associated with organized structure in boundary layers. Here they are identified as possible analogs of the inertial-range inverse cascade (backscatter) and the effects of the fluctuating rate of forward cascading, respectively. Further investigations to delineate more clearly the origins and the circumstances of occurrence of such patterns are suggested.

DOI: 10.1103/PhysRevFluids.6.044611

I. INTRODUCTION

A basic feature of turbulent boundary layers is the leading-order influence of shear or imposed-pressure-gradient forcing of streamwise flow in the core region that induces turbulent transport of momentum toward the wall, while the wall itself is the momentum sink. Here it is proposed that this global picture can be extended by considering the wall-normal transport of a local fluctuation of the core-flow state. Unless the fluctuation entirely dissipates before reaching the wall, some influence of the original fluctuation will arrive at the wall after some time lag t^*. The wall stress could thereby be affected by a core-flow fluctuation that occurred in the past, inducing a time-lagged cross-correlation between the core flow and the wall stress.

Wall stress τ is defined as $\rho\nu u_y(y=0)$, where ρ and ν are the fluid density and kinematic viscosity, both assumed constant, and $u_y(y=0)$ is the wall-normal derivative of streamwise velocity u evaluated at the wall, hence at distance $y=0$ from the wall. In what follows, quantities are

*alan.kerstein@gmail.com

expressed in wall units by normalizing using the appropriate combinations of ρ, ν and $\overline{u_y}(y = 0)$, where the overbar denotes ensemble averaging. This is equivalent to streamwise averaging based on specialization here to fully developed flow, although the results are generally applicable to thin boundary layers to a good approximation.

The above-mentioned time-lagged cross-correlation would be reflected in single-time spatial cross-correlations as follows. The core-flow fluctuation not only spreads laterally but also is advected downstream at a speed that is roughly the mean streamwise velocity at the height of the fluctuation onset. That velocity is higher than typical velocities closer to the wall, so the fluctuation influence arrives at the wall at a streamwise location that is upstream of the concurrent location of the original fluctuation. This indicates the possibility of correlation between the wall-stress response and the core-flow fluctuation that induced this eventual response, which has meanwhile arrived at a location downstream of the affected wall location. Accounting for the range of possible heights of the original fluctuation and the height dependence of the streamwise velocity, any induced correlations between core-flow streamwise velocity and wall stress would tend to form an obliquely oriented ridge of peak correlation.

Such a correlation pattern has been observed experimentally in boundary layers at moderate [1] and high (geophysical scale) [2] Reynolds numbers, *Re*. (The definitions of *Re* that are applicable to the flows considered here are discussed in Sec. VII and references cited therein.) One focus of such studies is the identification and characterization of organized structures, which has been done in various ways, but for high *Re*, the only reported evidence is the spatial pattern of the cross-correlation between wall stress and streamwise velocity measured at various wall-normal and streamwise offsets in the atmospheric surface layer. That pattern conforms to the description in the previous paragraph, but the inferred causation was the presence of obliquely oriented organized structures rather than the wall-normal transport of fluctuations, where the latter does not invoke the presence of organized structure. Thus, there are two if not more possible interpretations of the correlation pattern, where the two identified interpretations are based on a structure and a process, respectively. Accordingly, the high-*Re* observation does not conclusively establish the presence of organized structures at high *Re*.

A process causation has been mentioned in Ref. [1], here denoted as BT, as a possible alternative explanation of particular correlation patterns. (It is noted below in Sec. VII that their proposed causation differs from the specific mechanism outlined above.) The context was the development of a measurement strategy that enabled the investigators to rule out explanations other than organized structure for the particular case they were investigating.

In the present study, flow processes devoid of organized structure that might induce oblique correlation patterns are examined both conceptually and through numerical simulation. The latter involves a variant of hierarchical parcel-swapping (HiPS), a stochastic model [3] that has been used to simulate fully developed turbulent channel flow [4], which is likewise the flow configuration used here.

The HiPS modeling concept is outlined in Sec. II. A modification of the previously described model formulation is introduced in Sec. III and the Appendix in order to obtain a definitively minimal representation of turbulent channel flow, followed in Secs. IV and V by a comparison of the performance of the previous and current versions. The focus of the present HiPS application is described in Sec. VI. Finally, the numerical study is presented in Sec. VII and discussed in Secs. VIII and IX.

II. THE HIPS MODELING CONCEPT

As originally formulated [3], HiPS is a mixing model that extends commonly used multiparcel models by introducing a minimal representation of the relative separation of parcel pairs. This involves a binary (or more generally a *p*-adic) tree structure with a parcel attached to each node at the base of the tree. This structure is introduced solely as a geometrical representation of

parcel-pair separation. The values of the state variables of the various parcels constitute the model representation of the physical state of the system.

Specializing to a binary tree, parcel pairs can mix only if they are adjacent in the sense that both parcels are linked to a common node one level higher than the base of the tree. In the simplest implementation, which is adopted here, each pair of adjacent parcels is deemed to be fully mixed, so the states of the two constituent parcels are identical.

Turbulence phenomenology is introduced through a process that involves the selection of two subtrees, both emanating from tree nodes at some chosen level of the tree, to be swapped. This affects the relative separations of parcels, but parcel adjacencies are modified only if the selected subtrees are two nodes at the base of the tree, each associated with an individual parcel. In this case, two pairs of newly adjacent parcels are formed. In each of these pairs, the two constituent parcels, which in general have different states prior to the swap, are fully mixed immediately upon execution of the swap, and thereby become identical in composition.

HiPS is used here as a turbulent flow model in which the parcel state consists of velocity components u (streamwise), v (wall-normal), and w (spanwise), here referencing the channel-flow configuration. (Density ρ is omitted because it reduces to a universal scaling factor for the constant-density flows considered here.) In this context, the limitation of parcel mixing to adjacent pairs indicates that the lowest (base) level of the tree is analogous to the Kolmogorov microscale at which viscous transport terminates inviscid inertial-range cascading.

Model features that enable quantitative representation of turbulence phenomenology are as follows. First, subtrees at a given level that are selected to be swapped cannot be arbitrarily positioned relative to each other. Rather, they must emanate from a common node two levels higher, which is termed the apex of the swap. This enforces a degree of proximity of the two subtrees such that the swap is a reasonable idealization of the turnover of a turbulent eddy. Second, the mean frequency at which a given subtree pair is swapped is specified in accordance with an estimate of the turnover time of the corresponding turbulent eddy based on the current instantaneous state of the flow as specified by the collection of parcel velocities. Owing to this dependence on the flow state, the swapping frequency varies with time, with a different time variation for each subtree pair that is eligible to be swapped. Third, each swap is deemed to be the first of two operations constituting an eddy event, where the second operation is modification of parcel velocity components to reflect orientational redistribution of kinetic energy during a turbulent eddy motion, thus incorporating return-to-isotropy phenomenology.

The details of the continual time variation of the swapping frequencies, which are the main physical content of the model, and other model features have been fully described [4]. That reference also describes specialized features of the model that enable simulation of turbulent channel flow. For this case, the parcels are deemed to be aligned in the wall-normal direction, representing a notional line of sight spanning the channel height. The first and last parcels are attached to the respective walls, so their states are fixed at zero velocity. This is enforced by resetting a wall parcel to zero velocity each time it mixes with its adjacent parcel, which is an exception to the equality of the states of adjacent parcels. All other parcels are subject to a constant rate of linear-in-time increase of streamwise velocity based on a specified mean pressure gradient, as well as the swapping and mixing operations that modify parcel wall-normal locations and parcel states, respectively.

III. REDUCED HIPS CHANNEL-FLOW FORMULATION

The introduction of wall parcels whose states are fixed in time at $u = v = w = 0$ introduces inhomogeneity into the otherwise statistically homogeneous model. Proximity to a wall is determined by the highest tree level that is reached by the unique direct path (i.e., the path with no backtracking) from a given parcel to either wall, where proximity is low if the direct path reaches a high level. There are many more parcels than tree levels, so the parcels can be partitioned into groups such that the parcels in each group are equidistant from the closest wall, here meaning that they have the same proximity to that wall. The time histories of the states of parcels that are equidistant from the

closest wall are statistically equivalent. For example, the mean velocity profile is piecewise uniform, as shown in Fig. 2 of Ref. [4]. Accordingly, reported results were based on averaging within each statistically equivalent group.

The proximity criterion implies that each group corresponds to the set of parcels at the base of some subtree. In a binary tree, the number of parcels at the base of a subtree is some power of 2. Starting from a wall, the succession of statistically equivalent groups corresponds to a sequence of subtrees that each originate one level higher than the previous subtree, so the number of parcels per group doubles in each successive group from the wall to the channel midpoint. Thus, the number of parcels is exponentially larger than the number of groups, implying a potentially huge simplification, and commensurate cost reduction, if the HiPS formulation is reduced to one evolving state per group rather than per parcel.

To accomplish this, the formulation must be modified in a manner that limits its scope of applicability. The approach is illustrated by retaining all parcels but modifying the mixing rule. Instead of mixing only newly adjacent parcel pairs, which are formed only by lowest-level eddy events, all the parcels in any statistically equivalent group that has nonidentical parcels after an eddy event of any size are fully mixed. An exception to this rule is that mixing across the channel midpoint is excluded, so the two statistically equivalent groups that meet at the centerline do not mix. (This simplifies the mathematical implementation of group mixing, which is explained in the Appendix.)

On this basis, the parcels in each group are not only statistically equivalent, but identical at all times. Then the system state is always piecewise uniform as in Fig. 2 of Ref. [4], but with varying values of (u, v, w) in each uniform interval as the system evolves. Accordingly, the system state is fully specified by a set of evolving states $S_g = (u_g, v_g, w_g)$, each of which is the state common to all parcels at a given instant in the group labeled by index g.

In conjunction with the swapping rules, this implies that there can be at most two distinct parcel states in a statistically equivalent group immediately after a swap. If there are two, then owing to the doubling of the number of parcels in each successive group, half of the parcels in the group are in each state after the swap. This allows the final state of the fully mixed group to be expressed as a linear function of the preswap states of the two affected parcel groups and the postswap velocity changes applied during the eddy event. Details of this direct determination of the final system state based on the initial system state and the eddy-event specification are explained in the Appendix. This avoids sequential implementation of the eddy event and the mixing, which would prevent the reduction of the system state to the set of group states S_g. A visual rendering of the application of the procedure to a representative swap followed by group mixing is shown in Fig. 1.

The set of states S_g is likewise sufficient for implementing the other operations on the system, namely the pressure-gradient forcing and the wall treatment (which consists of setting $u = v = w = 0$ in a wall parcel after any mixing with its neighbor). The system state representation needed to time advance the simulation has thus been reduced from the set of parcel states to the exponentially smaller number of group states S_g.

IV. PHENOMENOLOGY OF THE REDUCED FORMULATION

Relative to the previously described model implementation [4], the reduced formulation can be viewed as a coarse-grained version involving box filtering of each statistically equivalent group of parcels. The filter width increases linearly with distance from the wall, albeit in discrete steps. In effect, the reduced formulation resolves only the local integral scale and is roughly analogous to Reynolds-averaged Navier-Stokes methods with respect to this particular feature. In this sense the reduced formulation is not a multiscale representation of turbulent flow although the hierarchical structure of the previous formulation is partially retained, as seen in Fig. 1.

As in any under-resolved fluid-dynamical computation, filtering and associated closure modeling are most effective when the goal is to capture mesh-resolved behavior. This approach sacrifices subfilter information that might be of intrinsic interest, where a common remedy for this is to

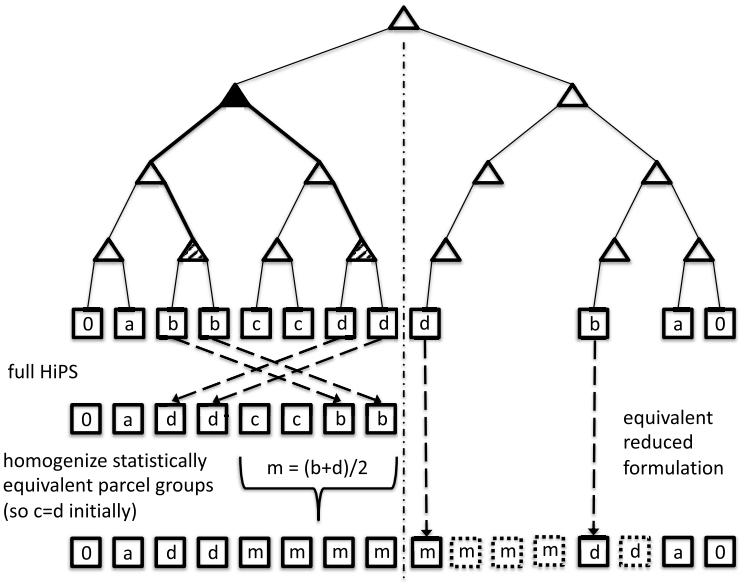

FIG. 1. The implementation of a representative swap illustrates the difference between the full and reduced HiPS channel-flow formulations. A five-level tree is shown. In full HiPS, there are 16 parcels at the base of the tree, but only the eight left-of-center parcels (squares) are shown. The equivalent reduced formulation is shown to the right of the vertical dashed-dotted line that separates the two halves of the flow domain. In full HiPS, a pair of adjacent parcels has the same state (schematically, b, c, or d) because adjacent parcels mix instantly if any operation produces adjacent parcels with different states. Whenever the leftmost pair is mixed, the wall parcel is then reset to $u = v = w = 0$, denoted as state 0, to enforce the wall boundary condition, but its nearest neighbor remains at some different state a. The tree structure (triangles and line segments connecting them) identifies allowed swaps, adjacent parcel pairs, and statistically equivalent parcel groups, which are collections of parcels with the same proximity to the nearest wall parcel. The filled triangle is the apex of the illustrative swap and the apex of each swapped subtree is denoted by a striped triangle, where thick line segments denote the paths from the former to each of the latter. Associated parcel displacements, indicated by dashed arrows, yield the modified system state as illustrated. Below that, additional operations corresponding to reduced HiPS are shown. In reduced HiPS, all parcels in a statistically equivalent group are fully mixed, so c and d must be equal initially. This implies that the group of parcels whose states are (c, c, b, b) mix to identical states (m, m, m, m), as shown. This enforced uniformity of parcel groups allows each group to be represented by one parcel, as shown right of center in a mirror-image rendering of the left-of-center operations. Parcels thus omitted have dotted borders. As explained in the Appendix, an eddy event consists of a swap followed by an additional operation that is not illustrated in the sketch, requiring generalization of the indicated algebraic expression for m.

introduce subfilter modeling of the excluded phenomena. By analogy, the full HiPS implementation can be viewed as the subfilter extension of the reduced version for the purpose of resolving the turbulent cascade and any associated case-specific phenomenology within each group of statistically equivalent parcels.

HiPS can be applied to homogeneous turbulence and some free shear flows [3]. In the former case, all parcels are statistically equivalent, so the entire system is one homogeneous parcel group that is not embedded within any larger-scale process. Hence the reduced formulation as implemented here has no role in this case, but it might be applicable to free shear flows as well as some buoyancy-driven configurations.

One effect of filtering is the suppression of the contribution of state fluctuations within statistically equivalent groups to single-point fluctuation statistics such as the velocity variance.

TABLE I. Simulation cases. Case F is the previously reported [4] case N9 and case R refers to present results. Re_τ is the friction Reynolds number, t^+ is the simulation time in wall units, and CPU is the processing time of the run. CPU/t^+ is expressed in seconds.

Model	Re_τ	t^+	CPU	CPU/t^+
Full (F)	1967	249262	66 min	0.016
Reduced (R)	1882	5963370	40 sec	0.0000067

Single-point fluctuations are large-scale dominated, which somewhat mitigates the effect of this artifact. Its effect is assessed quantitatively in Sec. V.

HiPS channel-flow results have been compared to measurements and direct numerical simulations of fully developed turbulent channel flow [4]. For this configuration, the unique determination of all single-time statistics requires one external input, the channel-flow friction law. (The parameter A representing the multiplicative length-scale stride from level to level also affects results, but as previously explained [4], $A = 0.5$ is the uniquely preferable choice because it corresponds to the desired effective dimensionality $d = 1$ of the parcel array.) On this basis, wall-normal profiles of the velocity mean and variance and the cross-stress $\langle u'v' \rangle$ were predicted, as well as the terms of the turbulent kinetic energy budget and the probability density function of the wall stress. Predictive capability that is unprecedented for such a highly simplified model was demonstrated.

The reduced HiPS application reported here corresponds to the baseline case of that study. In Sec. V, the reduced formulation is shown to be in generally close agreement with previous HiPS results. The exception is the velocity variance because, as anticipated, the filtering effect reduces fluctuations. The resulting variance reduction somewhat improves the overall agreement with measurements. On this basis, it is concluded that for the channel-flow characteristics that were previously examined, the fidelity of the two formulations is roughly the same.

V. DEMONSTRATIONS OF THE PERFORMANCE OF THE REDUCED FORMULATION

Comparisons of results obtained using the current reduced formulation of HiPS and the previous formulation are presented. The same case setup is used for both formulations, but as shown in Table I, they correspond to different Re_τ values. This is because, in the absence of viscous advancement in a literal sense, viscosity is inferred from the mean velocity gradient and the mean momentum flux at the wall. The resulting 4% difference between the two Re_τ values is one indication of the sensitivity of results to the difference between the two formulations.

Figure 2 shows the Reynolds shear stress for the two cases. For this and the figures that follow, format, normalizations, and details of the data reduction conform to the previous treatment of the full formulation [4]. Because the only viscous transport is by the surrogate mechanism of enforcement of the no-slip boundary condition at the walls, the linear behavior expected in the advection-dominated region away from the wall is obeyed, with an abrupt fall to zero at $y = 0$, corresponding to viscous dominance. The agreement of case R with these dependences is precise, while case F exhibits slight deviations due to the finite though long (in wall units) duration of the simulation. Case R ran for a much longer time in wall units, which was sufficient to eliminate any discernible deviation from linearity away from the wall.

The much longer physical run time of case R corresponds to much less CPU time than for case F, reflecting a reduction in run time per unit physical time by more than three orders of magnitude. The dependence of the number of degrees of freedom on Re_τ is logarithmic for reduced HiPS but a power law for full HiPS, indicating that the cost reduction will be even more dramatic for higher turbulence intensities of practical interest. This should be weighed against the progressive loss of resolution with increasing distance from the walls, which would be acceptable for some but not all applications.

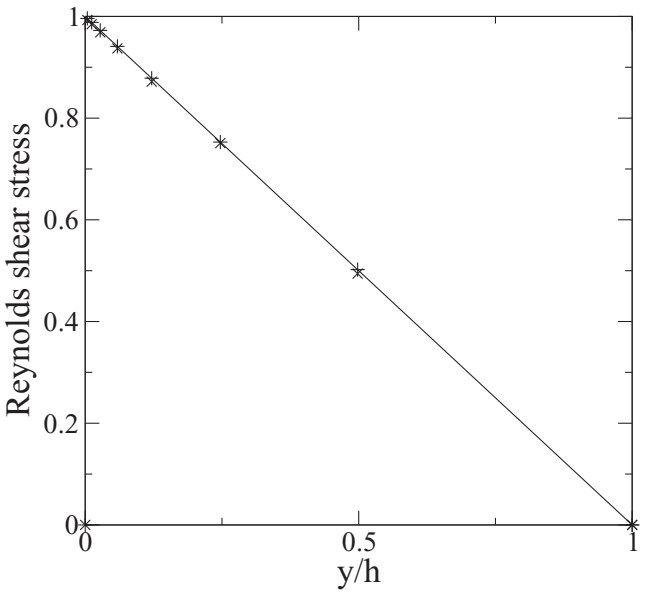

FIG. 2. Absolute value of wall-normalized Reynolds shear stress for Table I cases: +, case R; ×, case F; ——, exact result in the absence of viscous transport. Distance y from the wall is normalized by the channel half-height h.

The results that follow include the same comparisons to measurements and/or direct numerical simulation (DNS) results as previously [4]. This provides an indication of the impact of case differences on model accuracy.

The features of the HiPS mean velocity profile relative to measurements, shown in Fig. 3, were previously explained. The figure shows no significant differences between cases R and F, hence no loss of accuracy relative to case F.

As anticipated in Sec. IV, Fig. 4 shows that suppression of spatial variations within statistically homogeneous zones cause a reduction of velocity variances. The overall effect is to improve agreement with measurements. This cannot be attributed to better physical modeling because the sole effect of the model modification on results is to remove physically valid behavior. Nevertheless, it implies a preference for the reduced formulation on the pragmatic basis of improved accuracy.

Notwithstanding the effect of model reduction on fluctuation statistics, Fig. 5 shows that it has negligible effect on the turbulent-kinetic-energy (TKE) budget. The previous evaluation of the HiPS TKE budget showed negligible dependence on Re_τ, so the comparison to a DNS result for lower Re_τ is justified. The reproduction of the DNS result with overall good accuracy by the reduced formulation establishes a new milestone with regard to accurate prediction of the channel-flow TKE budget using a minimal model.

The probability density function (PDF) of wall stress, shown in Fig. 6, highlights the improved statistical precision resulting from running case R to much higher t^+ than case F was run. Based on t^+ values and CPU times in Table I, case F would have required tens of hours of run time to achieve comparable precision. This is not prohibitive for laboratory scale flows, but the reduced formulation is uniquely affordable for, e.g., geophysical scale flows.

Within the uncertainty of the case F results, Fig. 6 indicates that the two formulations are in agreement. The comparison to a DNS result for lower Re_τ is justified because it was previously shown that the HiPS wall-stress PDF is insensitive to Re_τ.

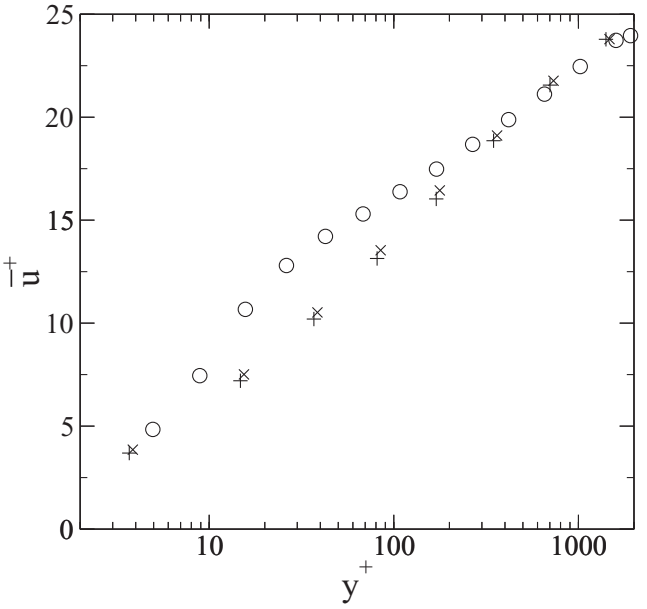

FIG. 3. Mean velocity profile in wall-normalized coordinates: +, case R; ×, case F; ◯, measurements for $Re_\tau = 2000$ [5].

VI. HIPS ANALOG OF SPATIAL CROSS-CORRELATIONS

HiPS channel-flow simulations temporally evolve velocity profiles along a wall-normal line of sight. Thus they can generate only time-lagged cross-correlations between points on such a line.

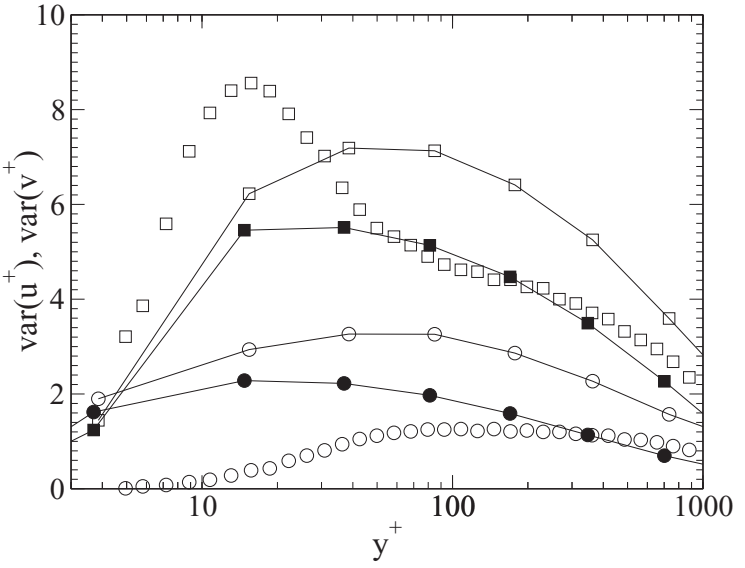

FIG. 4. Velocity variances $\overline{u'^2}^+$ (□) and $\overline{v'^2}^+$ (◯) for cases R (filled symbols) and F (open symbols), connected by lines for both cases. The symbols not connected by lines are measurements for $Re_\tau = 2000$ [5].

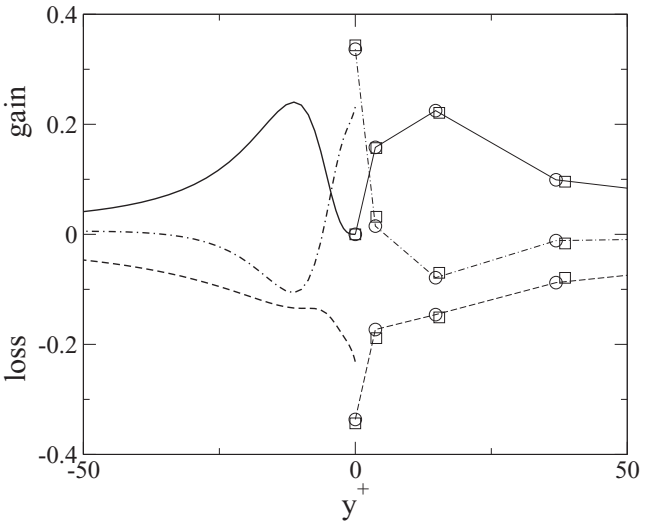

FIG. 5. Positive y^+: TKE budget, normalized by u_τ^4/ν: ◯, case R; □, case F. Negative y^+: DNS for $Re_\tau = 590$ [6]. Budget terms: ——, production; − − −, dissipation; − · −, sum of viscous and advective transport.

Therefore the present approach is to generate such time-lagged cross-correlations and then invoke the scenario described in Sec. I, supported by the results of BT, to draw inferences about the single-time x-y spatial correlation pattern.

That scenario is sharpened by considering the relationship of the time-lagged cross-correlation between wall stress τ and u at some distance Y from the wall, both measured at the same streamwise station x, to the single-time spatial pattern in the x-y plane of the correlation between τ and u. Such a relationship was inferred by BT from measurements of both quantities.

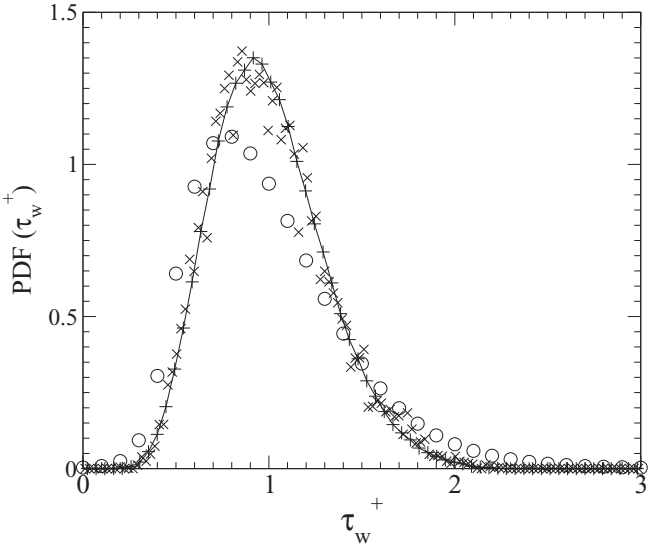

FIG. 6. PDF of wall-normalized wall stress: +, case R; ×, case F; ◯, DNS for $Re_\tau = 1000$ [7]. The curve connecting the case R symbols shows the smoothness of the PDF for that case.

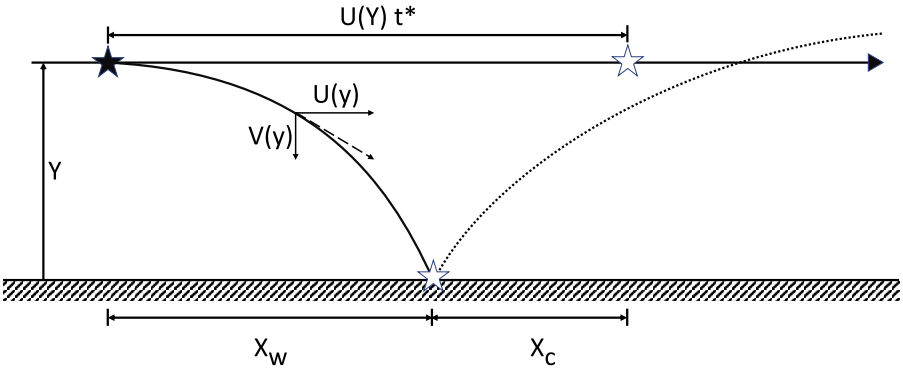

FIG. 7. Sketch of the propagation of the influence of a fluctuation originating at a nominal time $t = 0$ at height Y above the wall (filled star). After a time t^*, it has arrived at the wall at a distance X_w downstream of its origin and concurrently advanced a distance $U(Y)t^*$ directly downstream of its origin (open stars). At a representative point on the trajectory toward the wall (solid curve), the velocity vector tangent to the trajectory (dashed) is decomposed into its streamwise and downward components $U(y)$ and $V(y)$, respectively. As explained in Sec. VII, the resulting near-wall perturbation at time t^* can initiate reverse (upward, downstream) propagation (dotted curve).

Importantly, the relationship between the two statistical quantities is the same whether the correlations reflect spatial structure or a process as described in Sec. I. This reflects the broader point that the physical interpretation of these statistical quantities and their relationship is not unique, as emphasized by BT.

A simple picture that idealizes the process interpretation is formulated. This is done by assuming, as in Sec. I, that a fluctuation at some distance Y from the wall is advected downstream at the mean velocity $U(Y)$. After a time lag t^* the fluctuation influence arrives at the wall. At that moment, the wall stress τ is correlated with the fluctuation that originated earlier (by an amount t^*) at height Y.

On this basis, the current (time t^* after fluctuation inception) streamwise separation X_c of the correlated locations is estimated. Relative to its inception point, the fluctuation is advected a distance $U(Y)t^*$ downstream. (Here it is assumed that the fluctuation persists while being advected.) During the time t^* it also spreads laterally toward the wall with some notional leading-edge velocity $V(y)$. Integrating $dy/dt = V$ and noting that V is negative, this gives $t^* = -\int_0^Y dy/V(y)$. Additionally, as the leading edge advances laterally downward, at each height y it is advected downstream at a velocity $U(y)$. Expressing the time increment dt as $dy/V(y)$, $X_w = -\int_0^Y dy\,U(y)/V(y)$ is obtained, where X_w is the streamwise separation between the fluctuation inception point and the point of its impingement on the wall. Finally, the streamwise separation between X_w and the current (time t^*) streamwise location of the height-Y fluctuation is $X_c = U(Y)t^* - X_w$. These relationships are illustrated in Fig. 7.

Note that X_w/t^* is a weighted average of $U(y)$ in $[0, Y]$. Because U is an increasing function of distance y from the wall, where for the channel this applies up to the half-height h, its weighted average X_w/t^* in $[0, Y]$ is less than $U(Y)$, showing that $X_w < U(Y)t^*$. Therefore $X_c > 0$, i.e., the locus of the most highly correlated pairs of locations is tilted downstream relative to the wall.

The weighted average X_w/t^* can be expressed as some representative value $U^*(Y)$ of $U(y)$ in $(0, Y)$. Focusing on the logarithmic sublayer, $U(y)$ is a slowly varying function of y, so for given Y, $U^*(Y) = k(Y)U(Y)$ for some $k(Y) < 1$ of order unity. This yields the relation $X_w = k(Y)U(Y)t^*$. BT provides information pertinent to estimation of $k(Y)$.

Using the same time origin as above, the time $t(Y)$ at which the fluctuation at height Y arrives at the the streamwise location X_w relative to the fluctuation inception point is $X_w/U(Y)$. The foregoing results imply that $t(Y) < t^*$. Following the notational convention of BT as explained

in Sec. VII, $t(Y) - t^*$ is denoted T, where $-T$ is the time lag from passage of location X_w by the streamwise-advected fluctuation at height Y until wall impingement of the fluctuation at location X_w. Accordingly, $-T$ is the time lag for which the wall stress and the flow fluctuation at height Y, both evaluated at streamwise station X_w, should be most strongly correlated. Conversely, the observed maximum of this correlation as a function of T identifies the nominal arrival time of the height-Y fluctuation at location X_w.

If the functions $k(Y)$ and $V(y)$ could be determined or estimated, which might be possible using full-field data that three-dimensional numerical simulations can provide, then a direct one-to-one relationship between the time-lagged statistics and single-time x-y correlation patterns could be established. This is neither possible based on presently available data nor is it the present goal. Rather, the physical picture that has been outlined based on the stated assumptions is intended as a semi-quantitative elaboration of the discussion in Sec. I. Similar reasoning, albeit differing in some details, can demonstrate an analogous relationship between the spatial and temporal perspectives based on streamwise advection of organized large structures, reflecting the ambiguity noted by BT.

VII. CROSS-CORRELATION RESULTS

A channel-flow simulation using the model formulation described in Sec. III is used to evaluate the time-lagged correlation coefficient

$$R_{\tau u}(T) = \langle \tau'(t) u'(Y, t+T) \rangle / \sqrt{\langle \tau'^2 \rangle \langle u'^2(Y) \rangle}, \tag{1}$$

where angle brackets denote time averages, primes denote mean-subtracted values and the plus sign is used for consistency with BT. Results are compared to measurements of $R_{\tau u}(T)$ at a fixed streamwise location. The comparison is interpreted in terms of the physical picture outlined in Sec. VI.

As noted in Sec. IV, the only external input needed in order for HiPS to uniquely predict all single-time statistics for fully developed channel flow is the friction law. This is because the sequence of flow states is fully specified but an adjustable model parameter that rescales time by controlling the swap frequency remains undetermined. Multitime statistical input is needed to calibrate this parameter and thereby enable evaluation of the needed time-lagged cross-correlation. BT report statistics fully analogous to those produced by the HiPS simulation, so the time axis of the HiPS output is scaled to bring the results into conformance with the measurements. Figure 8 shows the resulting comparison.

Although the statistical quantities are fully analogous, the same cannot be said for the flow configurations. The HiPS results are for fully developed channel flow but the measurements were performed in a spatially developing turbulent boundary layer at a streamwise station corresponding to momentum-thickness Reynolds number $Re_\theta = 10160$. For consistent comparison to channel data, the empirical relation $Re_\tau = 1.13 Re_\theta{}^{0.843}$ [8] is used to obtain the equivalent friction Reynolds number $Re_\tau = 2700$.

Re_τ is an output rather than an input for a given specification of the HiPS channel flow configuration that includes the empirical friction law as input [4]. Specifically, Re_τ is uniquely determined by the chosen number of tree levels. The choice for the present application is 10 levels, corresponding to $N = 9$ for N as previously defined [4]. The resulting value of Re_τ is 1882. This differs from the value 1967 shown in Table I of that reference, reflecting the difference between the previous HiPS formulation and the present reduced formulation.

The HiPS results shown in Fig. 8 are obtained from a simulated flow realization that ran for a time interval $t^+ = 6 \times 10^6$ in wall units. The first half of that time interval allowed for relaxation to statistical stationarity and the statistical output was gathered during the second half. As an indication of how reduced the model is, this simulation ran in 40 sec on a commodity serial processor. Excluding the degenerate wall parcels, this is based on 16 parcels spanning the channel, hence 48 degrees of freedom based on three velocity components. (For present purposes, using only the u component would have given equally relevant results, reducing the number of degrees of

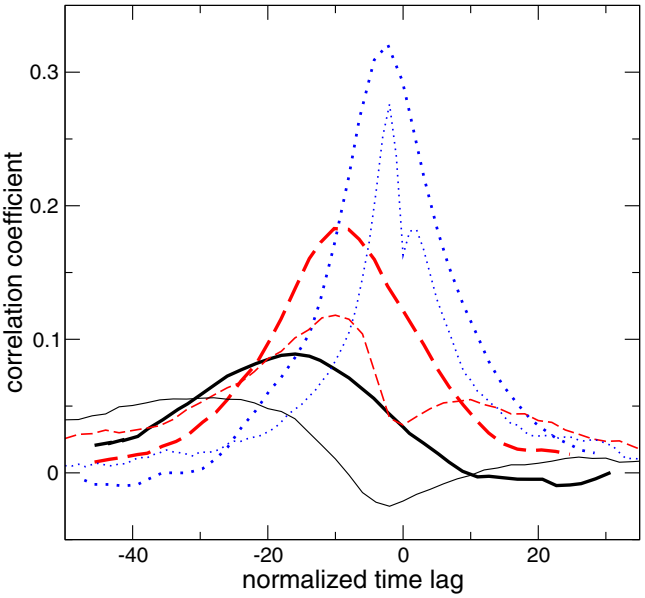

FIG. 8. Correlation coefficient specified by Eq. (1). Time lag is normalized by δ/U_0, where δ is the boundary-layer thickness and U_0 is the free-stream velocity. Thick lines, boundary-layer measurements by BT; thin lines, model channel-flow results with time lag scaled for consistency with the measurements using the same scaling factor for all model profiles. Height Y in Eq. (1), normalized by the half-height h for the channel flow and by δ for the boundary layer: blue dotted, $Y/h = 0.04$, $Y/\delta = 0.05$; red dashed, $Y/h = 0.18$, $Y/\delta = 0.25$; black solid, $Y/h = 0.37$, $Y/\delta = 0.50$.

freedom to 16. However, the intent here is to use a formulation that is equivalent to the previous HiPS channel-flow formulation, except for homogenization of statistically equivalent zones, so as to isolate the effect of that modification on model results.)

An individual parcel in the reduced HiPS formulation corresponds to a parcel group in the full HiPS formulation. The full formulation defines the relationship between the parcel array and the flow geometry, so reflecting this, the Y value of a reduced parcel is taken to be the geometrical midpoint of the parcel group that it represents. The Y/h values shown in the caption of Fig. 8 were determined on this basis. There is thus no freedom to choose Y values directly corresponding to the boundary-layer data. In any case, this correspondence is not easily defined because Y is normalized by different quantities for the two flows. Accordingly, some Y values for which the HiPS results are representative of the range of measured behaviors were chosen for presentation in the figure.

As noted, BT measured the single-time spatial correlation pattern as well as the time-lagged cross-correlations shown in Fig. 8 and thereby demonstrated that the leftward shift of the peaks of the time-lagged cross-correlations corresponds to a downstream-inclined ridge in the spatial correlation pattern. This determination supports the interpretation of the HiPS results in terms of the spatial correlation pattern in the x-y plane as outlined in Sec. VI.

The main features of the HiPS cross-correlations are the leftward shift and diminution of the peak of the cross-correlation with increasing Y, which are consistent with the measured trend. The only tuning done in generating this plot is horizontal scaling of the model results, so the model is strictly predictive with regard to the peaks of the cross-correlation curves. If the relationship $h = 2\delta$ is assumed, then the combined model and experimental results imply monotonic dependence of peak height on Y/δ. Here, δ as conventionally defined is the y value at which the mean streamwise velocity is 99% of the specified free-stream (large-y) value U_0. (Future comparison of model results to cross-correlations obtained from DNS of channel flow is desirable in order to circumvent the imprecise

relationship between the two flows considered here.) However, the broader point, irrespective of the degree of quantitative agreement, is that a specific instantiation of a process-based mechanism that reproduces key measured trends has been demonstrated. The definitively minimal stochastic model formulation excludes any possible influence of organized structure on the simulation results.

This point is further broadened by examining features of the model results that have not previously been noticed but suggest several extensions of the conceptual picture outlined in Sec. VI. One such feature is the sequence of secondary cross-correlation peaks seen at positive time lags, shifting rightward with increasing Y. This suggests the occurrence of wall stress fluctuations at some instant whose influence propagates laterally, thereby inducing fluctuations at successively larger Y values and consequent correlation signatures that are strongest at the positive time lag T from their initiation until their arrival at Y. [Note that the sign of T in Eq. (1) determines the direction of causality.]

A mechanism that might produce this behavior is as follows. The pressure and shear forcings in boundary layers occur predominantly in the core flow. Wall-stress fluctuations are then driven by the lateral transport of these fluctuations toward the wall, thus producing the primary sequence of cross-correlation peaks that has been noted. These wall-stress fluctuations are subject to dissipation and thus weakened but not fully eradicated. The weakened fluctuations can initiate the propagation of fluctuation influence back toward the core flow, resulting in the secondary ridge in the correlation pattern that is indicated by the model results in Fig. 8. This propagation of fluctuation influence from the forcing zone to the dissipation zone, inducing a weaker reverse propagation, is reminiscent of the turbulent-kinetic-energy flow in scale space in the inertial-range cascade, so this picture is termed the cascade analogy. In this context, the reverse flow is termed backscatter. It is represented schematically by the dotted curve in Fig. 7.

Terminology aside, this picture is substantively clarifying. For example, BT proposed that the alternative to the organized structure interpretation of the primary sequence of peaks seen in Fig. 8 is "events at the wall being convected out into the flow," but as noted, this requires cross-correlation peaks at positive rather than negative T. The cascade analogy supersedes such anecdotal and in this case implausible interpretations by providing a consistent unitary picture of the relationship between correlation patterns and boundary-layer phenomenology.

Notwithstanding this clarification, the question remains whether the backscatter mechanism in fact occurs in boundary layers. The measurements provide some relevant evidence. The $Y/\delta = 0.50$ cross-correlation profile approaches zero with positive slope at a normalized time lag of 30, indicating that it then becomes positive. It must eventually return to zero, indicating that a secondary peak must exist. Because this feature is subtle and was not the focus of the experimental study, there is no assurance that it is statistically significant or free of bias. However, it is noteworthy that a cross-correlation profile measured at $Y/\delta = 0.75$ (omitted from Fig. 8 for clarity) exhibits a similar tendency. Additionally, the $Y/\delta = 0.25$ profile exhibits an apparent inflection point near normalized time lag 18 that suggests the incipient emergence of a secondary peak at larger Y/δ. Collectively, the model results, experimental evidence, and physical reasoning suggest that gathering additional relevant evidence experimentally (e.g., by extending measurements to larger normalized time lags) or using DNS could provide useful insight.

Even if the predicted secondary ridge is verified, the fact remains that the model is not quantitatively accurate in this regard. One possible reason for this model result to be less accurate than model results for single-time statistics is that treatment of the lateral line of sight as a closed system results in permanent streamwise alignment of fluid parcels at all heights. This can induce larger cross-correlations than occur in the physical flow because physical fluid parcels are in streamwise alignment only for a limited time owing to the lateral variation of the streamwise velocity. This constrained opportunity for lateral interactions among fluid parcels inhibits the development of cross-correlations relative to the model.

This reasoning similarly applies to the primary ridge. The somewhat better accuracy of the prediction of this feature might reflect the fact that the physical cause of that measured feature is known by other means to be an organized structure rather than the mechanism captured by the

model, so the model could be reproducing the feature by means of a different mechanism. Indeed, this ambiguity of causation is one of the points illustrated by the model.

Bimodal profiles necessarily have a local minimum between the peaks, as seen in the $Y/\delta = 0.50$ measured profile as well as in the model results. However, the minimum is not required to be at negative correlation, and indeed is at positive correlation for two of the model profiles. The model shows successively deepening minima with increasing Y/h, culminating in a negative minimum.

The cascade analogy indicates how a negative minimum might arise. Just as turbulence intensity fluctuations can modulate the rate of downscale energy transport in the inertial-range cascade, fluctuations of turbulence intensity in the channel-flow simulation can modulate the rate of momentum transfer toward the wall. Reduced momentum transfer can allow more time for pressure-induced core-flow acceleration prior to lateral transfer of the accelerated fluid toward the wall, resulting in a positive core-flow streamwise velocity excursion. Reduced lateral momentum transfer also implies reduced compressive straining of the near-wall flow, hence a reduction of wall stress. Higher-than-average momentum transfer reverses both effects. These considerations imply negative $R_{\tau u}$. This mechanism is likely to be most effective for large Y, consistent with the trend indicated by the model results and suggested by the measurements, which exhibit the onset of negative $R_{\tau u}$ for $Y/\delta = 0.50$. There does not appear to have been any prior attempt to explain this behavior.

This reasoning is based on modulation of the turbulence intensity somewhere within the y range $[0, Y]$ for given Y. Although the effects at the wall and at $y = Y$ are roughly concurrent and therefore affect the cross-correlation at zero nominal time lag, there can be a deviation depending on whether the effect of a modulation is felt sooner at $y = 0$ or $y = Y$. For small Y, the effects at both locations should be felt rapidly so the local minimum of the time lag should be close to lag zero, while for larger Y there is more freedom for the minimum to deviate from zero time lag. This tendency is indicated by the model results in Fig. 8. The measurements suggest a larger deviation of opposite sign. The sign and magnitude of the deviation are sensitive to subtle details of the spatial distribution of modulation occurrences and the speed at which their influence propagates to $y = 0$ and $y = Y$, respectively, so it is plausible that the highly simplified model is not quantitatively predictive in this regard.

Deviation here refers to the mean deviation seen in the time-averaged correlation function. However, the deviation is different for each modulation occurrence and inferences can be drawn concerning the range of variation of the deviation. A small (large) range of variation implies that the local minimum of the correlation function is sharp (shallow). For small Y, the effect of a modulation occurrence is felt quickly at both 0 and Y, so the possible time difference between the effects at the two locations is constrained accordingly. For large Y, the delays until the modulation occurrence is felt at the two locations can be longer so there is more scope for their difference to be large, implying a shallow minimum of the correlation function. This in fact is the trend indicated by the model results. (The measurements neither support nor contradict this finding.) It is concluded that the mechanism proposed to account for negative $R_{\tau u}$ values is consistent with all relevant features of the model results as well as with turbulence phenomenology more broadly, and it remains to be determined whether it is an observable feature of turbulent boundary layers.

Collectively, the noted observations indicate that the cascade analogy is both an internally consistent framework and consistent with the available, albeit limited, evidence. It remains to be clarified whether it is uniquely consistent in these respects and whether the associated phenomenology is physically realized in some situations. Possible steps toward obtaining these and related clarifications are discussed in Sec. IX.

VIII. PERSPECTIVE

Notwithstanding the focus here on the cascade-analogy concept and its possible observable consequences, the context of the present study in terms of boundary-layer phenomenology more generally, and models thereof, merits some elaboration. As noted in Sec. IV, the simplification

TABLE II. Features of hierarchical boundary-layer-modeling approaches.

Model	Multiscale?	Dynamic?
HRAP	Yes	
Reduced HiPS		Yes
Full HiPS	Yes	Yes

of the full HiPS model to its reduced form suppresses its multiscale character. This eliminates possible structural influences of the multiscale character of the full model in order to facilitate an unambiguous interpretation of model results. In a broader context, this simplification has additional implications as follows.

Although the model remains hierarchical in the sense that parcel interactions are still specified by a (reduced) tree structure—see Sec. III and Fig. 1—the multiscale turbulent cascading captured by the full model is eliminated. This emphasizes that the cascade analogy is in fact nothing more than an analogy. In particular it does not invoke turbulent cascading *per se*, although physically there will be cascade influences at a more detailed level. Additionally, the elimination of turbulent cascading from the HiPS modeling framework addresses a broader point. Namely, it is shown in Sec. V that the reduced formulation accurately reproduces high-order statistics such as the TKE budget and wall-stress PDF whose insensitivity to multiscale phenomenology is not self-evident. This implies that a minimal time-accurate representation of unsteady boundary-layer dynamics is in some aspects more determinative than multiscale cascading with respect to statistical properties.

This inference is tempered by the noteworthy performance of the hierarchical random additive process (HRAP), recently reviewed in Ref. [9], which involves a purely stochastic (vs dynamical) treatment of multiscale phenomenology in turbulent boundary layers. Unlike full multiscale HiPS but like other multiscale hierarchical models (see Ref. [3] for discussion and references), the statistics of the resolved streamwise velocity u at y are based on independent identically distributed random contributions from successively coarse-grained eddies, where the degree of coarse-graining determines the range of y values over which an eddy contributes to $u(y)$. The number $N(y)$ of contributions at given y is based on a simple mixing-length picture. Motivated by a hierarchical picture of organized boundary-layer structure, the contributions are additive, in contrast to typical multiplicative formulations intended to represent the homogeneous inertial-range turbulent cascade [10,11]. This approach reproduces a variety of high-order single-point and multipoint fluctuation statistics of $u(y)$ and related quantities such as the wall stress.

Reduced HiPS cannot reproduce all these properties, which are understandably sensitive to the multiscale character of turbulent boundary layers. A more interesting possibility is that full HiPS might have such capability. This will be investigated in the future. The interplay among various modeling approaches might clarify the respective influences of organized structure, multiscale phenomenology, and flow dynamics on the various statistical properties of turbulent boundary layers. In particular, there is a precise mathematical relationship between the HiPS tree structure and the HRAP formalism that allows the physical parcel states generated during HiPS simulations to be transformed into the direct analog of the summands in the HRAP prescription for evaluation of $u(y)$ statistics. This suggests potentially instructive comparisons of full HiPS and HRAP with respect to the statistical properties of the summands as well as the physical predictions of the two approaches, with possible implications regarding structural vs process origins of observed behaviors.

A schematic comparison of the respective approaches is provided in Table II. Notably, the dynamical character of HiPS embodies an underlying physics representation that not only affects the physical interpretation of results but also enables its application to a broader class of boundary-layer regimes, including a variety of transient situations that are beyond the scope of formulations that are predicated on statistically stationary multiscale phenomenology.

IX. DISCUSSION

The model results shown in Fig. 8, complemented by the cascade analogy conceptual framework outlined here, suggest several novel dynamical features of boundary layers whose experimental signatures can be gleaned from the available experimental data. The cascade analogy is a process-based interpretation of observed cross-correlation patterns rather than a structure-based interpretation, but this does not rule out the possibility that the constituent processes are mediated by spatially organized events. For instance, the outward propagating wall events corresponding to backscatter in present terminology could be highly structured bursts that are prevalent near-wall features, as noted by BT. Thus, the relevant dichotomy is between correlation patterns that reflect organized structure *per se* and patterns induced by processes that might or might not be mediated by organized motions.

Notwithstanding previous recognition of the possible process-based origins of such observations, this possibility has not previously been addressed systematically nor received much attention. As noted in Sec. I, the persistence of organized structure at high Re was reported [2] to be established by cross-correlation measurements that were not supported by evidence ruling out a process-based interpretation. The present study identifies plausible process-based scenarios and their observable signatures, thereby potentially aiding in the design of diagnostics that could establish their presence or absence.

The computational model employed here is formulated to be devoid of organized structure by construction. The minimal treatment enables a focus on the most elementary notional instantiation of boundary-layer dynamics. For this and other noted reasons, it is not quantitatively accurate, yet it exhibits remarkable features, the secondary correlation ridge and the occurrence of negative correlation, that are natural corollaries of the cascade analogy. Importantly, the cascade analogy is a synthesis of known phenomenology rather than a hypothesis about new physics, so it has sound physical underpinnings notwithstanding the novelty of its implications. Those implications are supported, albeit tentatively, by the available experimental evidence.

The latter point leads to the main conclusion of this investigation. The cascade analogy provides guidance with regard to future studies that might provide more definitive assessments of the tentatively identified boundary-layer processes. Some possibilities have been mentioned. Another is conditional sampling, which was shown by BT to be useful for discriminating among interpretations of correlation patterns. In the present context, the conditioning strategy could be reversed, i.e., conditioning could be used to isolate regions devoid of organized structure rather than maximally influenced by organized structure. It has been demonstrated computationally [12] that organized structures are increasingly sparse as Re_θ increases and that the background flow is relatively featureless, hence the background flow is especially promising for conditioned numerical assessment of the cascade analogy.

APPENDIX: DETAILS OF THE REDUCED MODEL FORMULATION

The details of the present reduction of the previously reported HiPS channel-flow formulation are explained. As explained in Sec. II, the instantaneous flow state is specified by the collection of parcel states. To simplify notation, parcel states are denoted by a scalar v, which represents any of the three velocity components.

In Sec. III it is noted that flow evolution equivalent to the reduced formulation, but numerically less efficient, is obtained by retaining the full HiPS state representation in terms of parcels rather than groups but mixing all parcels within any group that contains parcels with nonidentical states after an eddy event. The algebraic representation of this procedure is formulated, leading to a direct representation of the post-event system state in terms of the preswap group states v_g, here referring to parcel-group values of the scalar v. This enables efficient time advancement of the reduced formulation using only the collection of group states v_g.

Two equal-size subtrees are swapped, where one corresponds to a group labeled 1 consisting of N parcels with group state v_1 and the other is contained in a group labeled 2 consisting of $2N$ parcels

with group state v_2. Group 1 is an N-parcel subtree and group 2 contains two N-parcel subtrees, one of which is involved in the swap. The constraints on allowed swaps in the channel-flow configuration [4] require that all swaps are of this type except swaps that cross the channel midpoint. As mentioned in Sec. III, the latter type of swap involves a pair of statistically equivalent groups that are not treated as a single group and therefore are not homogenized after this type of eddy event. Nevertheless, each of the groups comprising that pair is itself homogeneous and its homogeneity is restored after any eddy event that swaps parcels in from another group.

After the swap involving the illustrative groups 1 and 2, the state of all group-1 parcels is v_2 and group 2 consists of equal numbers of state-v_1 and state-v_2 parcels. Swapped parcels are subject to the additional eddy-event operation that redistributes kinetic energy among velocity components while conserving momentum. For a given event, this involves adding a velocity increment denoted c to the group-1 parcels and $-c$ to the parcels swapped into group 2, where c is a specified functional of the three velocity components in each of the two affected groups based on physical modeling considerations [4]. (Constant density is assumed, so momentum conservation requires that the sum of all changes of a velocity component is zero, as enforced by the equal and opposite increments $\pm c$.)

Group 1 thus remains homogeneous with the new group state $v_1' = v_2 + c$. Group 2 now has equal numbers of state-$(v_1 - c)$ and state-v_2 parcels. Homogenization of group 2 by mixing all parcel states gives the new group state $v_2' = \frac{1}{2}(v_1 + v_2 - c)$.

These results are sufficient to specify the reduced formulation, but data reduction introduces an additional consideration. The evaluation of budgets, e.g., of turbulent kinetic energy, requires identification of the respective contributions of advective and dissipative processes [4]. The HiPS eddy event consists of a swap and subsequent $\pm c$ incrementation of parcel velocities, which are advective operations, followed by mixing of one of the participating groups (group 2 in the representative example), which is dissipative. The specific quantities that need to be extracted during each eddy event include the mean A of advection-induced parcel-property changes and the mean B of the advection-induced changes of the square of each parcel property. Likewise, the mean D of dissipation-induced parcel-property changes and the mean E of the dissipation-induced changes of the square of each parcel property are needed.

Eddy events dissipate property fluctuations due to averaging over parcel states within a group. This averaging evaluates the group mean v_g without modifying it, so the mean change induced by this averaging is $D = 0$. However, the induced mean change E of the squared parcel properties can be nonzero, as indicated below.

For group 1, the foregoing results give $A = v_1' - v_1 = v_2 - v_1 + c$ and $B = v_1'^2 - v_1^2 = (v_2 + c)^2 - v_1^2$. This group is not subject to mixing and hence there is no dissipation, so E as well as D is zero. For group 2, the nonzero contributions are $A = \frac{1}{2}(v_1 - v_2 - c)$, $B = \frac{1}{2}((v_1 - c)^2 - v_2^2)$, and $E = \frac{1}{4}(v_1 + v_2 - c)^2 - \frac{1}{2}((v_1 - c)^2 + v_2^2) = -A^2$. These relations suffice for computation of the contributions of eddy events to the turbulent-kinetic-energy budget shown in Sec. V. The contributions resulting from enforcement of the wall boundary condition are the same as in the full HiPS formulation.

Almost all the eddy events in a high-Re simulation using the full HiPS formulation involve subtree pairs contained within a statistically homogeneous group. These eddy events are eliminated in the reduced formulation because an eddy event applied to a collection of identical parcels has no effect. The increased efficiency of the reduced formulation is due to the huge reduction of the number of implemented eddy events and the associated reduction of the frequency at which eddy events are randomly sampled. The reduction of sampling frequency is an important benefit because eddy sampling is done by oversampling successive candidate eddies and rejecting most of them. This involves a mathematical procedure in which candidate eddies are generated based on rough estimation of their propensity but are selectively rejected so as to enforce the physically based eddy statistics. To exploit this additional efficiency gain, the candidate eddies that are sampled in the reduced formulation are restricted to be those that swap subtrees in different groups.

[1] G. L. Brown and A. S. W. Thomas, Large structure in a turbulent boundary layer, Phys. Fluids **20**, S243 (1977).
[2] J. P. Monty and M. S. Chong, A review of recent investigations into high Reynolds number wall-turbulence, in *COSnet/CSIRO Workshop on Turbulence and Coherent Structures in Fluids, Plasmas and Nonlinear Media*, edited by J. Denier and J. S. Frederiksen (World Scientific, Singapore, 2007) World Scientific Lecture Notes in Complex Systems, Vol. 6, pp. 227–246.
[3] A. R. Kerstein, Hierarchical parcel-swapping representation of turbulent mixing. Part 1. Formulation and scaling properties, J. Stat. Mech. **153**, 142 (2013).
[4] A. R. Kerstein, Hierarchical parcel-swapping representation of turbulent mixing. Part 2. Application to channel flow, J. Fluid Mech. **750**, 421 (2014).
[5] M. P. Schultz and K. A. Flack, Reynolds-number scaling of turbulent channel flow, Phys. Fluids **25**, 025104 (2013).
[6] R. D. Moser, J. Kim, and N. N. Mansour, DNS of turbulent channel flow up to $Re_\tau = 590$, Phys. Fluids **11**, 943 (1999).
[7] P. Lenaers, Q. Li, G. Brethouwer, P. Schlatter, and R. Örlü, Rare backflow and extreme wall-normal velocity fluctuations in near-wall turbulence, Phys. Fluids. **24**, 035110 (2012).
[8] P. Schlatter and R. Örlü, Assessment of direct numerical simulation data of turbulent boundary layers, J. Fluid Mech. **659**, 116 (2010).
[9] X. I. A. Yang and C. Meneveau, Hierarchical random additive model for wall-bounded flows at high Reynolds numbers, Fluid Dyn. Res. **51**, 011405 (2019).
[10] A. S. Gurvich and A. M. Yaglom, Breakdown of eddies and probability distributions for small-scale turbulence, Phys. Fluids **10**, S59 (1967).
[11] K. R. Sreenivasan and G. Stolovitzky, Turbulent cascades, J. Stat. Phys. **78**, 311 (1995).
[12] P. Schlatter, Q. Li, R. Örlü, F. Hussein, and D. S. Henningson, On the near-wall vortical structures at moderate Reynolds numbers, Eur. J. Mech. B/Fluids **48**, 75 (2014).